RESEARCH PAPER

Pre-Identification Data Merging for Multiple Setup Measurements with Roving References

H. Ceylan [1] · **G. Turan** [1] · **Ç. Hızal** [1]

Abstract

One-time operational modal analysis (OMA) of large civil structures requires measurements of the vibrations, which, according to the number of channels to be measured, are generally expensive and arduous to obtain. In this study, identification of modal parameters of civil structures has been investigated by using multiple setups with a roving reference channel. In this manner, a limited amount of equipment becomes sufficient for OMA of structures. The procedure consists of a transformation function between measurement setups, which transforms all measured data to the time frame of a selected reference setup. To illustrate the procedure, an existing 10 story laboratory shear frame model is considered. A numerical and an experimental investigation have been carried out to identify its modal characteristics. The validity of the procedure has been explained in detail by making use of a coherence function in-between the multi-setup measurements. According to the results, OMA by using only a few sensors with the performed procedure can be equivalent to OMA by using a full measurement setup. Against a common believe, the results of this study reveal that synchronization among the setups does not prominently affect the identification results.

Introduction

OMA of large civil structures such as bridges requires measurements of the vibrations, which are generally arduous to obtain. Response measurements have been obtained with wired communication for years and today it is also possible to acquire such measurements with wireless communication by means of ongoing technological developments in wireless sensors. In the case of wired communication in long structures, environmental noise is very likely to enter the measured response signals. This means that acquired response measurements could not represent the actual structural response behavior when long signal cables are used. One way to reduce the noise in long cables is to use multiple data acquisition systems in the structure and have shorter distances to the sensors. In the case of wireless connections, all wireless sensors cannot communicate with a central data acquisition unit since wireless communication bandwidth is very limited. Thus,

several data acquisition units need to be set up to acquire measurement data from distant sensors that are placed within a long or tall structure [1]. To overcome this problem, electronic component manufacturers focus on low energy sensors and battery systems which may be charged by environmental radio frequency (RF) signals.

The usage of large number of sensors requires large number of channels on data acquisition systems. In addition, multi-centered data acquisition units further increase the cost for both wired and wireless communication. If the measurement system is only going to be placed onto the structure for the purpose of a one-time single measurement and removed afterwards; the installation and the management of the various components should be carefully designed.

When multiple setups of sensors are employed, each setup is obtained at a different time and due to a different excitation. Because of this reason, each setup becomes unsynchronized with the other one. By reviewing the literature, it is seen that these unsynchronized data can be used for the identification of modal frequencies and damping ratios, however using unsynchronized data makes the identification of global mode shapes of structures impossible unless a merging strategy is applied before, during or after the identification process. In order to apply a merging procedure between the setups, they have to

✉ H. Ceylan
    hasanceylan@iyte.edu.tr

[1] Civil Eng. Department, Izmir Institute of Technology, Izmir, Turkey

share at least one common sensor. This sensor is called the reference sensor between two setups and generally this (or these) sensor(s) is/are left stationary during all measurements. While a fixed-positioned reference sensor for all setups is used for many applications, roving reference sensors are also used for system measurements.

In the literature, there are numerous studies that consider the different merging strategies for multiple setup applications. Peeters and Guido [2] have combined the stochastic subspace identification (SSI) with the idea of using reference sensors in multiple setups. In their methodology called SSI/ref., the information on the reference sensor data has been inserted in the identification step. They have tested a steel transmitter mast by using three fixed-positioned reference sensors with a total of 4 setups. High prediction errors have been obtained for non-reference channels and therefore they have concluded that the modal shape estimates are less reliable. In a similar manner, Reynders and Roeck [3] have proposed a reference-based version (CSI/ref) of the combined deterministic-stochastic subspace algorithm (CSI) by using a Kalman filter of the reference outputs. They have implemented their proposed methodology on the Z24 bridge in Switzerland and very accurately identified the first 14 modes which have been the most complete set by that time. They have concluded that these two methodologies are one of the most powerful methods for EMA and OMAX analysis.

Van der Auweraer et al. [4] have focused on the inconsistency in the data acquired by multiple setups for the large-scale tests of complex structures. In their study, it is observed that the effects of bias errors on the data are more important than the measurement noise and variance errors. Bias errors may be caused by wrong signal processing of the data and more importantly by multiple setups. In multiple setup applications, the data may be inconsistent due to the mass loading effects of transducers, temperature differences and changing boundary conditions from setup to setup. This may result in a frequency shift and the identification of multiple close modes from each setup instead of a single mode. Further, mode shape amplitude and phase errors may also arise when a large number of setups are employed. To reduce the errors in such problem, it is recommended that the sensors in each setup should be uniformly distributed over the structure in which each segment has similar mass and inertia. Further, all modes should appear almost in all setups. They have proposed to perform the identification for each setup separately, combine the results of each setup by correcting the shifted parameters and merge the partial modal parameters to the global ones. In addition, they emphasized the automation of the multiple setup analysis since a lot of user interference is required otherwise. At this stage, it is mentioned to use finite element models that can significantly contribute to the identification of true modes in an automated manner.

Döhler et al. [5, 6] and Reynders et al. [7] have some reviews and implementations of these strategies as pre- and post-identification data merging. They compare three different approaches (PoSER, PoGER and PreGER) that are used to obtain global modal parameters. These approaches differ from each other based on the order of data merging, normalization and system identification. In the PoSER approach, modal parameters are firstly identified for each setup separately. Modal frequencies and damping ratios identified from each setup are averaged and modal shapes of each setup are merged by using the reference sensor data to have global modal shapes. The authors have reached a result that the PoSER approach, which requires a system identification process for each setup, is not suitable for large number of setups and especially for OMA tests. In the PoGER approach, correlation functions or power spectral density (PSD) functions between all output signals and the reference signals are obtained for each setup separately. Then, the global modal parameters are obtained by adding the correlation or PSD functions on top of each other. This procedure requires the mode shapes to be re-scaled. On the other hand, in the PreGER approach, a global PSD matrix is constructed by merging the obtained PSD functions from each setup. PSD functions are scaled to a reference PSD to obtain the relation of all outputs with the reference one. Then, this global PSD matrix is employed to identify the global modal parameters. PoGER and PreGER have been found to be fast and less tiresome since the identification step is processed only once for the merged global system.

Mevel et al. [8] have proposed a merging strategy that is covered by the PreGER approach. They have proposed a time domain technique to deal with non-stationary data. In their technique, the Hankel matrix, which includes the correlation functions, is constructed for each setup. Each Hankel matrix is the factorization of the controllability and observability matrix. Since the excitation information of each setup is only included in their controllability matrices, they are removed from the Hankel matrix of each setup and replaced with a controllability matrix that is common to all setups. Then, the resulting Hankel matrices are merged into a global Hankel matrix and global modal parameters are identified by a subspace identification technique.

Brownjohn [9] has used a merging procedure that employs the spectral density functions. The merging operation is performed by evaluating the ratio of the cross-spectral densities of the measured signals within each setup to the auto-spectral density of the reference signal. Modal characteristics of two office towers have been identified by using the merging procedure with a common reference sensor in the frequency-domain peak-picking and NExT-ERA methods. Similarly, Siringoringo and Fujino [10] have performed a merging procedure which involves a time synchronization of the cross-correlation functions. They have used a single reference channel and 121 measurement points which correspond to 121

setups to measure the response of a plate. The synchronization among the setups is performed by a factor that is the ratio of the auto-spectral density functions of the reference channel. The synchronized cross-correlation functions have been employed in NExT-ERA to identify the modal parameters of the plate.

In this study, an extended approach of Brownjohn [9] and Siringoringo and Fujino [10] is used for the applications of OMA with multiple setups. The difference recites in the fact that the reference channel is not fixed. The setups have roving reference sensors, instead of common ones among all setups. The aim of this study is to investigate the accumulation of measurement errors which may occur due to the merging procedure between the setups in case of using roving reference sensors. A coherence function which has been proposed by Felber [11], Juang and Pappa [12], and Zhu and Au [13] has been employed in this study to observe the error accumulation after the merging process. The coherence function shows that the raw data among different setups are not coherent, whereas the transformed measurement data of the setups have high coherence values. The error in the obtained modal shapes is found to be related to the value of the coherence function. Thus, the outcome of this study is that dependable modal properties are obtained when the coherency among the data is high.

The measurement data obtained from the setups are merged before the identification step and then the merged global data is used in NExT-ERA to identify the global modal parameters [14]. Therefore, the performed methodology can be classified as a pre-identification merging strategy. The procedure has been performed on an existing 10 story laboratory shear frame model, and its numerical model. According to the results, the merged data of the measured multiple setups lead to the modal shapes and frequencies obtained from the eigenvalue analysis of the numerical model. The identified damping values are compared to the damping ratios that are calculated from a simple impulse response of the physical structure.

Methodology

Figure 1 shows a system measurement that consists of multiple setups, where each setup consists of a data acquisition system with five sensors. At least one sensor placement must be in common between two setups. Consequently, the sensor location is measured more than once, serving as a reference measurement that is used for the setup synchronization.

A similar approach to Brownjohn [9] and Siringoringo and Fujino [10] has been performed for the synchronization between multiple setups [14–16]. Let y_{ref}^i and y_{ref}^j be the acceleration responses which are measured by the reference sensor between setup i and j, and let $Y_{ref}^i(\omega)$ and $Y_{ref}^j(\omega)$ be the Fast

Fourier Transforms (FFT) of the acceleration response signals of y_{ref}^i and y_{ref}^j, respectively. A frequency dependent function is used to synchronize two setups. This function is evaluated to be the ratio of the FFTs of the reference channel measurement of setup i and j;

$$\alpha_{ij}(\omega) = \frac{Y_{ref}^i(\omega)}{Y_{ref}^j(\omega)} \qquad (1)$$

$\alpha_{ij}(\omega)$ is a frequency dependent function. It can be considered as a transformation function from measurement setup j to i. Similarly, the transformation function from measurement setup k to j becomes as follows;

$$\alpha_{jk}(\omega) = \frac{Y_{ref}^j(\omega)}{Y_{ref}^k(\omega)} \qquad (2)$$

Consequently, the transformation function from measurement setup k to i becomes as follows;

$$\alpha_{ik}(\omega) = \alpha_{ij}(\omega).*\alpha_{jk}(\omega) \qquad (3)$$

In eq. (3), ".*" represents the elementwise multiplication of two vectors. Then, the measurements of non-reference channels in setup j can be synchronized with the measurements in setup i as;

$$Y_{nonref^j}^i(\omega) = \alpha_{ij}(\omega).*Y_{nonref}^j(\omega) \qquad (4)$$

Similarly, the measurements of non-reference channels in setup k can be synchronized with the measurements in setup i as;

$$Y_{nonref^k}^i(\omega) = \alpha_{ik}(\omega).*Y_{nonref}^k(\omega) \qquad (5)$$

In eqs. (4) and (5), $Y_{nonref}^j(\omega)$ and $Y_{nonref}^k(\omega)$ represent the FFTs of the measurements of non-reference channels in setup j and k, respectively. Accordingly, $Y_{nonref^j}^i(\omega)$ and $Y_{nonref^k}^i(\omega)$ represent the FFTs of the measurements of non-reference channels in setup j and k, which have been synchronized with the measurements in setup i. Let $y_{nonref^j}^i$ and $y_{nonref^k}^i$ be the inverse FFTs (IFFTs) of $Y_{nonref^j}^i$ and $Y_{nonref^k}^i$, respectively. Then, $y_{nonref^j}^i$ and $y_{nonref^k}^i$ are the transformed time-domain measurements of non-reference channels in setup j and k as if they are measured at the same time with the measurements in setup i.

If a large number of setups are present, which are lined up in a series, the cumulative error in the transformation function

Fig. 1 A representative sensor placement for a multiple setup measurement system
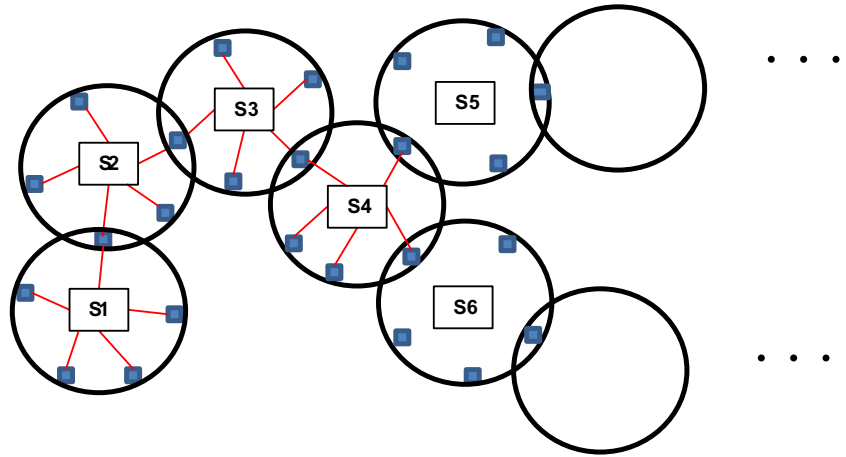
may limit the usage of this suggested procedure. As an example, the transformation function between setup #6 and setup #1 can be written as follows;

$$\alpha_{16} = \left(\frac{\overline{Y}^1_{ref\,12} + W^1_{ref\,12}}{\overline{Y}^2_{ref\,12} + W^2_{ref\,12}} \right) \cdot \left(\frac{\overline{Y}^2_{ref\,23} + W^2_{ref\,23}}{\overline{Y}^3_{ref\,23} + W^3_{ref\,23}} \right)$$
$$\cdot \, \ldots\ldots \cdot \left(\frac{\overline{Y}^5_{ref\,56} + W^5_{ref\,56}}{\overline{Y}^6_{ref\,56} + W^6_{ref\,56}} \right) \tag{6}$$

where the subscript "*ref ij*" is the reference channel which is common for setup i and j.

The following is a parametric investigation of the effect of noise on the transformation function between two setups. Measured reference response signals in frequency domain can be decomposed into the actual responses and measurement noise as follows;

$$Y^i_{ref\,ij} = \overline{Y}^i_{ref\,ij} + W^i_{ref\,ij} \tag{7}$$

$$Y^j_{ref\,ij} = \overline{Y}^j_{ref\,ij} + W^j_{ref\,ij} \tag{8}$$

where $\overline{Y}^i_{ref\,ij}$ and $\overline{Y}^j_{ref\,ij}$ are the FFTs of the actual (total) acceleration responses, $W^i_{ref\,ij}$ and $W^j_{ref\,ij}$ are the FFTs of noise signals in the reference sensor between setups i and j, respectively. Here, the actual frequency-domain responses, $\overline{Y}^i_{ref\,ij}(\omega)$ and $\overline{Y}^j_{ref\,ij}(\omega)$, can be written in terms of acceleration transfer function, which is well-known in the structural-dynamics literature, as

$$\overline{Y}^i_{ref\,ij} = \lambda^{ij}_{1xn} H_{nxn} F^i_{nxN} \tag{9}$$

$$\overline{Y}^j_{ref\,ij} = \lambda^{ij}_{1\times n} H_{n\times n} F^j_{n\times N} \tag{10}$$

where $\lambda^{ij}_{1\times n}$ is a selection vector consisting of 0's and 1 to select the reference DOF between setup i and j. H_{nxn} is the acceleration transfer function, and $F^i_{n\times N}$ and $F^j_{n\times N}$ are the vectors of excitation signals of setup i and j in frequency domain, respectively. The subscripts represent the size of the corresponding term. Here, n is the total number of DOFs of the system and N is the length of the excitation signal in frequency domain. The acceleration transfer function, H_{nxn}, is defined as;

$$H_{n\times n} = \Upsilon_{n\times n}^{-1} \tag{11}$$

where the matrix Υ is written as

$$\Upsilon(\omega) = \left[M + \frac{C}{j\omega} - \frac{K}{\omega^2} \right] \tag{12}$$

where M, C and K are the mass, damping coefficient and stiffness matrices in a size of nxn, respectively. In Eq. (11), inverse of the matrix Υ can be evaluated as follows;

$$\Upsilon^{-1} = \frac{1}{\Delta} \Upsilon^{adj} \tag{13}$$

where Δ is the determinant of the matrix Υ and Υ^{adj} is the adjoint matrix of Υ.

Measured reference response signals can be rewritten by substituting eqs. (9) and (10) into eqs. (7) and (8), respectively, as;

$$Y^i_{ref\,ij} = \lambda^{ij}_{1\times n} H_{n\times n} F^i_{n\times N} + W^i_{ref\,ij} \tag{14}$$

$$Y^j_{ref}ij = \lambda^{ij}_{1xn} H_{nxn} F^j_{nxN} + W^j_{ref}ij \tag{15}$$

By substituting eq. (13) into eq. (11);

$$H_{n\times n} = \frac{1}{\Delta} \Upsilon^{adj}_{n\times n} \tag{16}$$

Then, substituting eq. (16) into eqs. (14) and (15);

$$Y^i_{ref\ ij} = \lambda^{ij}_{1 \times n} \left(\frac{1}{\Delta} \Upsilon^{adj}_{n \times n} \right) F^i_{n \times N} + W^i_{ref\ ij} \qquad (17)$$

$$Y^j_{ref\ ij} = \lambda^{ij}_{1 \times n} \left(\frac{1}{\Delta} \Upsilon^{adj}_{nxn} \right) F^j_{n \times N} + W^j_{ref\ ij} \qquad (18)$$

Rearranging eqs. (17) and (18), the following equations can be obtained;

$$Y^i_{ref\ ij} = \frac{1}{\Delta} \left(\lambda^{ij}_{1 \times n} \Upsilon^{adj}_{n \times n} F^i_{n \times N} + \Delta.W^i_{ref\ ij} \right) \qquad (19)$$

$$Y^i_{ref\ ij} = \frac{1}{\Delta} \left(\lambda^{ij}_{1 \times n} \Upsilon^{adj}_{n \times n} F^i_{n \times N} + \Delta.W^i_{ref\ ij} \right) \qquad (20)$$

The transformation function α_{ij} between the setup i and j is then written by substituting (19) and (20) into eq. (1) as;

$$\alpha_{ij} = \frac{\lambda^{ij}_{1 \times n} \Upsilon^{adj}_{n \times n} F^i_{n \times N} + \Delta.W^i_{ref\ ij}}{\lambda^{ij}_{1 \times n} \Upsilon^{adj}_{n \times n} F^j_{n \times N} + \Delta.W^j_{ref\ ij}} \qquad (21)$$

From the theoretical aspect, the second terms, $\Delta.W_{ref}$, in eq. (21) do not exist if there is no noise in the measured responses. Assuming that the excitation signals $F^i_{n \times N}$ and $F^j_{n \times N}$ in the first terms are exactly the same, α_{ij} is being a vector of 1's and multiplication in eq. (4) does not change the values of non-reference channels of setup j. In multi-setup implementations, however, the excitations and their levels always differ from setup to setup.

In real life applications, noise exists in the measured responses. Then, the second terms, $\Delta.W_{ref}$, in eq. (21) come into the picture. In this case, the determinant, Δ, approaches to zero at resonant frequencies of the system. As a result, the noise has a very limited effect on the transformation function, α_{ij}, at the resonant frequencies. Further, as the damping of the system increases, the value of Δ slightly diverges from zero at the damped resonant frequencies. It can be deduced here that a greater amount of noise accumulates for the modes with higher damping ratios.

The first terms in eq. (21) which involve the frequency-dependent adjoint matrix, Υ^{adj}, become zero as the measured reference DOF corresponds to a nodal point of a certain modal shape. Therefore, the selection of reference DOFs should be appropriately considered.

Further investigations are carried out on numerical and experimental data. In later sections, the effect of measurement noise is shown by means of a coherence function. There, it will be shown that the transformation function is affected by noise, but the expected influence of additive noise does not appear to be an issue at resonant frequencies.

Implementations of the Methodology

The aforementioned methodology has been implemented on an experimental model, and its numerical model. For the experimental implementation, an existing 10-story shear frame structure has been tested in the laboratory under wind loading. Before the experimental implementation, the numerical application of the methodology has been firstly performed on the numerical model to be able to investigate the factors affecting the merging procedure. A simple 10-story shear frame model has been constructed for the existing structure by using the Matlab® [17] program. Both the existing structure and its numerical model have been presented in Fig. 2. Numerical results are compared with experimental results. In the following subsections, numerical study is firstly explained, and then experimental results are discussed in detail.

Numerical Application

Numerical Model

The physical structure is modelled as a shear frame model because it is weak in the x-direction, strong in the y-direction, and the torsional effects can be neglected. The column dimensions of the physical structure vary along the height; in the first three stories the width is 29.1 mm, the following four stories have a width of 22 mm, and the top three-story columns have a width of 16.7 mm. The thickness of the columns is 1.4 mm and it is constant over the height. Each story has a height of 12 cm, and the total height of the structure is 132 cm. The calculated story stiffness values in the weak direction are shown on Fig. 2. Each story, 1, 2 and 3 have a stiffness of k_1, stories 4–7 have a stiffness of k_2 and the remaining stories have a stiffness of k_3. Since all parts of the structure are made of steel material, Young's modulus and unit mass are taken as E = 200 GPa and 7800 kg/m³, respectively. Each story level consists of a steel plate with dimensions of 200x150x11.5 mm, which corresponds to a mass of 2.69 kg. The physical structure and its constructed numerical model have been shown in Fig. 2.

The modal damping ratio of each mode has been determined from experimental impulse response data by using the Hilbert transform method. To do so, the physical structure has been excited by an impulse force, and the acceleration response of the 10th story has been measured. The impulse response has been transformed into the frequency domain and a bandwidth filter has been applied to obtain the response of the mode in consideration. The filtered frequency domain response has been transformed into time domain to obtain the free vibration response of that mode. This process is repeated to obtain the modal damping ratios of the first six modes. The free vibration responses of the first and second modes are presented with their calculated exponential functions in Fig. 3.

Fig. 2 10-story shear frame structure and its lumped-mass model
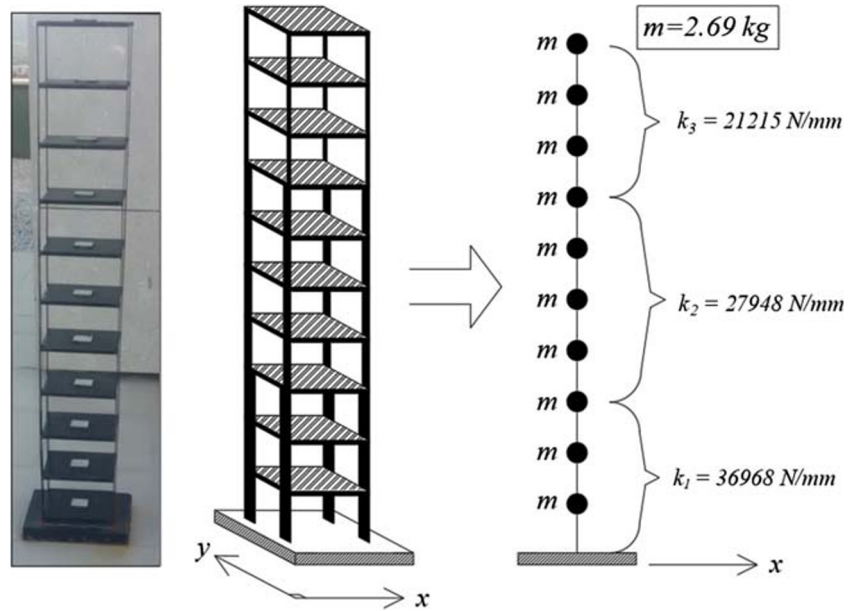
Modal frequencies obtained from the eigenvalue analysis of the numerical model and damping ratios obtained from the Hilbert method have been provided in Table 1. The frequencies are listed with four decimal place high precision to show the sensitivity of the performed merging procedure later in Table 2.

Generation of Response Data

The methodology has been tested on the numerical model that is described in the previous section. In this numerical investigation, measurements from the 10 DOF model are considered to be obtained by using three sensors only as shown in Fig. 4, which are then transformed to an equivalent full measurement set.

The numerical model has been excited by five different generic signals to have ambient vibration responses at different time intervals for each setup. For this purpose, five different

Gaussian white noise excitation signals with a duration of 15 min are generated. Here, the generated excitation signals have a sampling frequency of 1000 Hz. These white noise signals are different along the time line, but they are stationary signals which have a zero mean and unit standard deviation – statistically they are identical. For each setup, the excitation function has been applied to the stories by using the equivalent force of $F(t) = -\mathbf{M}\mathbf{1}\ddot{u}(t)$. Here, M is the mass matrix of the structure, $\mathbf{1}$ is the vector of ones and $\ddot{u}(t)$ is the excitation function. To simulate the wind loading, a random Gaussian white noise has been added into the excitation of each DOF to have a root mean square of 20% of the RMS of $F(t)$. Time history of the excitation signal of the 1st DOF in Setup #1 has been representatively provided in Fig. 5(a) with its auto-spectral density function in Fig. 5(b) in the Nyquist frequency band.

Five different simulations have been performed by using the Newmark-β method with the constant average
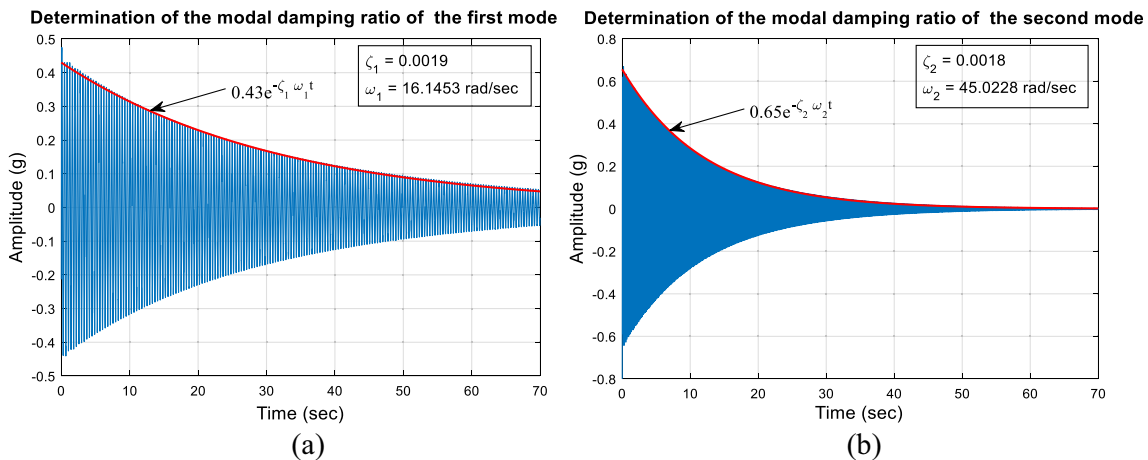
Fig. 3 Determination of the modal damping ratios for the first and second modes

Table 1 Modal frequencies and modal damping ratios of the numerical model

# Mode n	Modal Frequency, f_n (Hz)	Modal Damping Ratio, ξ_n
1	2.5696	0.0019
2	7.1656	0.0018
3	11.5929	0.0018
4	16.0195	0.0018
5	19.8201	0.0017
6	23.6266	0.0017
7	26.0085	–
8	28.3422	–
9	31.0699	–
10	34.6332	–

acceleration approach [18]. Measurements of the DOFs in each setup (Fig. 4) have been extracted from the corresponding DOF of the outputs. In addition, different random noise is added to each acceleration response signal in order to imitate the measurement noise effects as encountered in real life. To investigate the adverse effects of the amount of measurement noise on the performed methodology and identification process, and to observe the working performance limits, different noise levels have been included in the response signals until meaningful identification results could not be obtained. To this end, the noise is set for each acceleration response to have an RMS of 0, 50, 100, 200, 300, 500 and 1000% of the RMS of the response itself.

As a result, acceleration response of each DOF with different noise levels has been obtained as if the response data in a simulation are measured at a different time. Acceleration response data are obtained with a duration of 15 min and with a sampling frequency of 1000 Hz. In this study, it has been aspired to determine the first six modes of the model. Therefore, the acceleration response data were down-sampled to 50 Hz for a successful identification by NExT-ERA. Consequently, all the acceleration response measurements in the setups have been obtained with five different simulations in accordance with the sensor placement represented in Fig. 4.

All the acceleration response signals in the time domain have been transformed into the frequency domain by applying Fast Fourier Transforms (FFT). Setup #1 has been selected as the reference setup. Since the measurements in setup #1 are extracted from the full measurement set #1, the target is to estimate the response data which are equivalent to the response data obtained in the full measurement set #1. Therefore, all multi-setup measurements have been transformed to be the equivalent (synchronized) responses with the full measurement set #1. As representative ones, maximum singular value (SV) spectra of the acceleration responses

obtained from each setup having a measurement noise level of 0% have been presented in Fig. 6.

Identification Results of the Numerical Model

The synchronized response data have been implemented within an existing NExT-ERA algorithm to identify the modal parameters of the numerical model [19–23]. So as to visually inspect consistency of the true modes, stabilization diagrams have been plotted within the Nyquist frequency range for each identification process. As a representative one, Fig. 7 demonstrates one of the stabilization diagrams with reference channel 10 for the identification processes that are separately performed for each noise level. For visual comparison purposes, the auto-spectral density function of the 1st DOF for the noise level of 0% is located on the diagram with a scaling factor such that the peak amplitude is equal to the maximum model order. In the diagrams, specific frequencies show a high consistency when a different reference channel is selected for the identification process. The frequencies which are consistent in almost all the stabilization diagrams have the possibility of being the true modal frequencies. Final decision on the true modal frequencies has been made by calculating a modal assurance criterion (MAC) between the identified mode shapes that corresponds to the same modal frequency at a different solution with a different selection of model order. By using the orthogonality property of the modal shapes, mode shapes which have a MAC value of greater than 0.995 have been selected as being identical with each other and a basis vector of all these selected mode shapes has been calculated. The modal frequencies that correspond to the modal shapes included in the basis vector are also collected in a cluster. The highest MAC value between an identified mode shape and the basis vector has been determined and this identified mode shape is selected as the true mode shape of the numerical model and average of the modal frequencies in the corresponding cluster has been selected as the true modal frequency of the model [24].

In Table 2, the modal frequencies and modal damping ratios of the first six modes which have been identified by using the synchronized response data are compared with the modal frequencies obtained from the eigenvalue analysis and the damping ratios obtained from the logarithmic decrement analysis. According to the results, the first six modal frequencies of the model have been successfully identified with minor errors using the performed methodology for different levels of measurement noise.

Although some modal damping ratio identification results have minor errors within the acceptable limits, some others have major errors above the acceptable limits such as the first mode which has an error of 21% for the noise levels of 100% and 1000%. A large error in modal damping ratio estimation such as the case in this study is a well-known fact among

Table 2 Comparison of modal frequencies and damping ratios of the numerical model

# Mode	Noise Level (%)	Freq. (Hz) Eigenvalue analysis	Identified Freq. (Hz)	Relative Difference (%)	Actual Modal Damping Ratios	Identified Modal Damping Ratios	Relative Difference (%)
1	0	2.5696	2.5694	< 1	0.0019	0.0022	16
	50		2.5676	< 1		0.0022	16
	100		2.5674	< 1		0.0023	21
	200		2.5697	< 1		0.0022	16
	300		2.5712	< 1		0.0020	5
	500		2.5703	< 1		0.0021	10
	1000		2.5572	< 1		0.0023	21
2	0	7.1656	7.1634	< 1	0.0018	0.0020	11
	50		7.1639	< 1		0.0018	0
	100		7.1637	< 1		0.0019	6
	200		7.1626	< 1		0.0020	11
	300		7.1643	< 1		0.0019	6
	500		7.1653	< 1		0.0020	11
	1000		7.1757	< 1		0.0021	17
3	0	11.5929	11.5906	< 1	0.0018	0.0020	11
	50		11.5879	< 1		0.0018	0
	100		11.5933	< 1		0.0019	6
	200		11.5817	< 1		0.0017	6
	300		11.5860	< 1		0.0020	11
	500		11.5865	< 1		0.0019	6
	1000		-			-	-
4	0	16.0195	16.0087	< 1	0.0018	0.0019	6
	50		16.0028	< 1		0.0020	11
	100		16.0072	< 1		0.0018	0
	200		15.9924	< 1		0.0019	6
	300		16.0028	< 1		0.0017	6
	500		16.0164	< 1		0.0016	11
	1000		15.6934	2		-	-
5	0	19.8201	19.7819	< 1	0.0017	0.0019	12
	50		19.7932	< 1		0.0014	18
	100		19.7996	< 1		0.0014	18
	200		19.8007	< 1		0.0019	12
	300		19.7882	< 1		0.0015	12
	500		19.9048	< 1		0.0018	6
	1000		19.2407	3		-	-
6	0	23.6266	23.5823	< 1	0.0017	0.0018	6
	50		23.5839	< 1		0.0014	18
	100		23.5922	< 1		0.0015	12
	200		23.5812	< 1		0.0015	12
	300		23.5964	< 1		0.0019	12
	500		-			-	-
	1000		-			-	-

system identification researchers. Nayeri et al. [25] explained this problem as "modal damping estimation is always crude and not as accurate as the modal frequency estimation" in the system identification methods including NExT-ERA. In addition, Moaveni [26] observed that "the natural frequencies using different methods are reasonably consistent while the

Fig. 4 Placement of the sensors in each setup on the numerical model
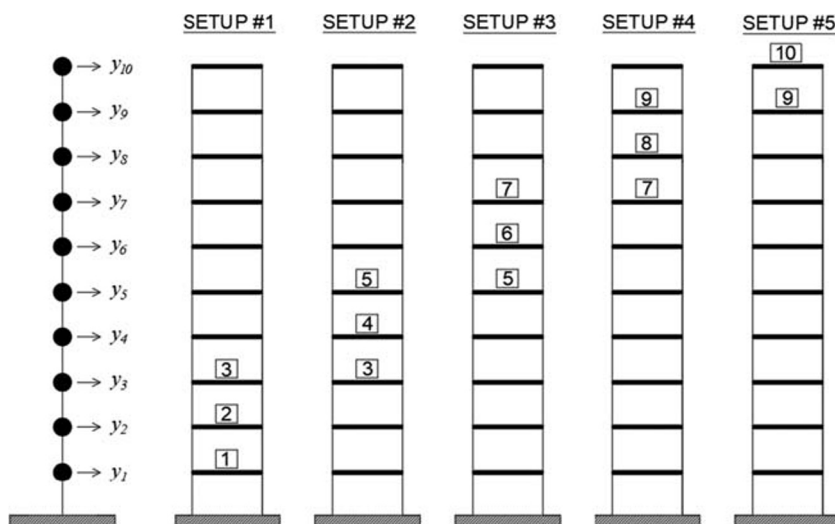
identified damping ratios exhibit much larger variability across system identification methods." Thus, it is arrived at the decision that major errors in identified modal damping ratios are independent from the implemented methodology in the identification process. Besides, the degrees of the modal damping identification results have a very good agreement with the results of the logarithmic decrement analysis. Since the damping values are very small numbers, such errors can be expected and accepted.

Identification process has been performed separately for each noise level by using the synchronized response measurements to identify the first six mode shapes of the numerical model. In addition to this, they have been identified separately for each noise level by using the full measurements. Both results have been compared with the mode shapes obtained from the eigenvalue analysis of the numerical model. Synchronization and full measurement results have been also compared to decide whether the identification results are affected by the measurement noise or the accumulated error in synchronization process. Comparisons of the first six mode shapes of the numerical model identified by using the synchronized response measurements are presented in Fig. 8,

and those identified by using the full measurements are presented in Fig. 9. To investigate the quality of the modal shapes in detail, MAC values have been calculated between the identified mode shapes and those obtained from the eigenvalue analysis, and the results have been presented in Table 3.

Coherency Investigation in-between Setups (Numerical Study)

The NExT-ERA method uses the correlation functions between the response signals. It is well known that there should be significant correlation between the measurements obtained from different DOF of the structure to identify the global mode shapes. Bearing this in mind, after the modal identification is performed, correlation levels between the response signals have been investigated before and after the synchronization process. To this end, it is seen that various coherence functions are suggested by researchers [11–13]. In this study, the square-root of the coherence function that is introduced by Felber [11] is employed. Here, the coherence function is defined as [13];
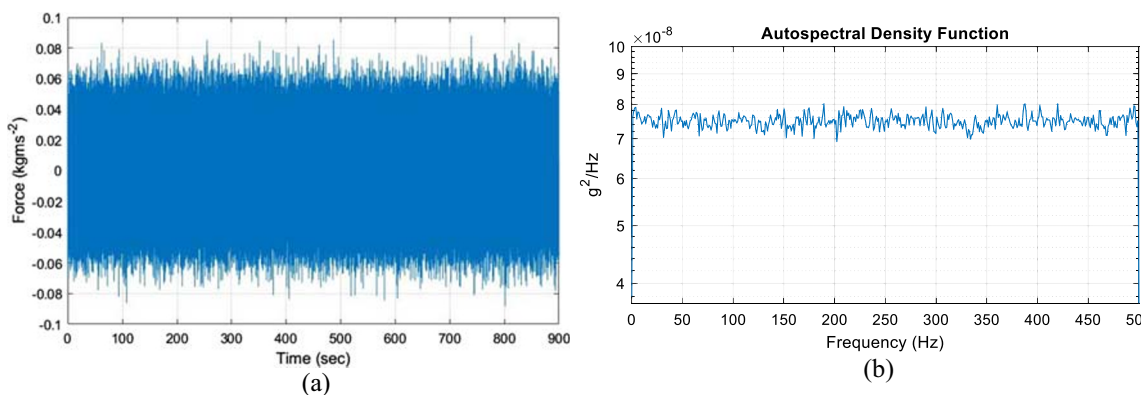

Fig. 5 (a) Time history of the excitation signal (for 1st DOF in Setup #1) and (b) its auto-spectral density function
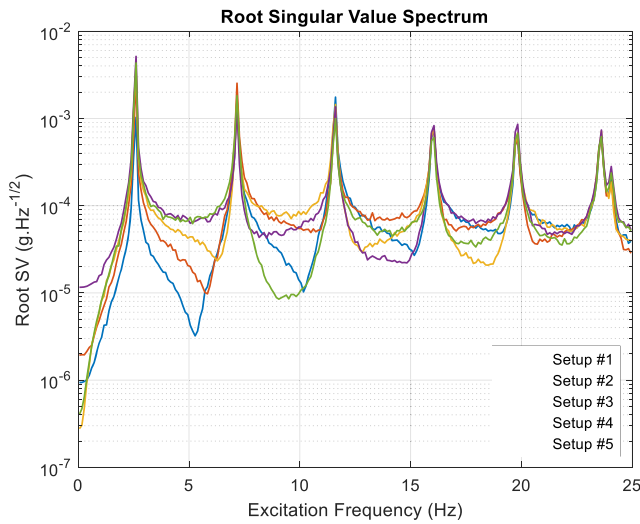
**Fig. 6** Maximum root-singular value spectra of each setup

$$\gamma_{ij}(\omega) = \frac{G_{ij}(\omega)}{\sqrt{G_{ii}(\omega)G_{jj}(\omega)}} \qquad (22)$$

where $G_{ij}(\omega)$ is the cross spectral density between the FFT signals, $Y_i(\omega)$ and $Y_j(\omega)$, and it is defined as;

$$G_{ij}(\omega) = Y_i(\omega)Y_j^*(\omega) \qquad (23)$$

in which $Y_j^*(\omega)$ is the complex conjugate of $Y_j(\omega)$. Similarly, $G_{ii}(\omega)$ and $G_{jj}(\omega)$ are the auto spectral densities of the signals $Y_i(\omega)$ and $Y_j(\omega)$, respectively. The absolute value of the coherence varies between 0 and 1. For the perfectly synchronous data, the absolute value of the coherency is defined as $|\gamma| = 1$ and for the perfectly asynchronous data, $|\gamma| = 0$ [13]. By using this definition, synchronized response signals by the performed methodology have been investigated from
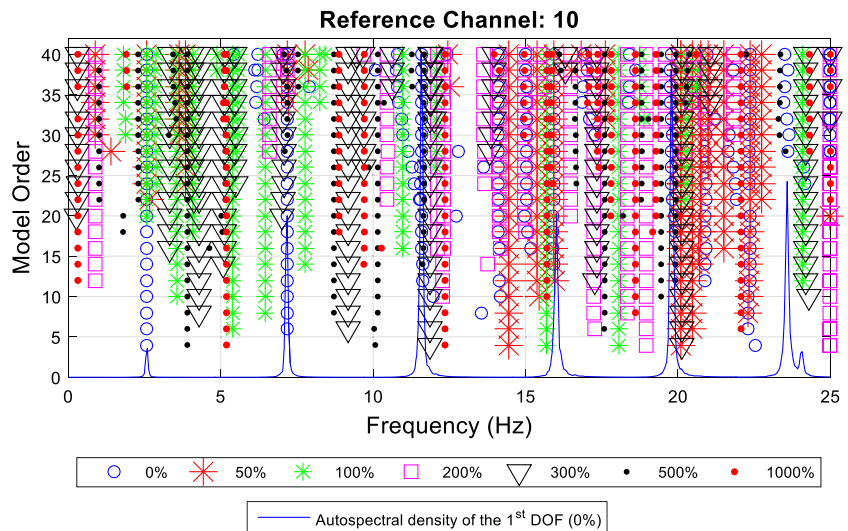
two different points of view for verification purposes. In the first investigation, the coherency between the synchronized signals and the corresponding DOF of the full measurement are presented. The second investigation shows the coherency between the signal of the 1st DOF and the synchronized signals of the remaining DOFs.

According to the first investigation, coherence values between the synchronized response signal of each DOF and the corresponding response signal of the full measurement set #1 have been evaluated. In Fig. 10, real parts of the evaluated coherence functions for selected DOF from the selected setups (4th DOF from setup #2 and 10th DOF from setup #5) have been presented over the Nyquist frequency bandwidth. Coherences that are calculated for response data with increasing levels of synthetically added random measurement noise (0, 50, 100, 200 and 300%) are also presented in the same figure. The results of higher noise levels (500 and 1000%) have not been shown on the figure for a clear view. Due to the noise density caused by the random excitation and measurement noise, high variation in coherence has been observed over the full range, except near the resonant frequencies. As seen from the coherence functions in Fig. 10, near the resonant frequencies the values are close to one for each selected DOF and for each level of measurement noise. As a common behaviour of the coherence function, it can be seen that the value is decreasing with the increase in noise level for the frequencies other than the dominant bandwidths. Further, the variance of the coherence is increasing with the increase in measurement noise level. These results prove the deductions that are made for the transformation of eq. (21) at the end of Section 2.

Since the identification have been performed at the dominant frequency ranges, a closer look is placed at the noise effect at the modal bandwidths. For this purpose, a mean value of the coherence has been estimated for the first six modes at a narrow resonant frequency band to be able to assess the

Fig. 7 A representative stabilization diagram within the Nyquist frequency range

**Fig. 8** Comparison of the first six mode shapes of the numerical model (obtained by multiple setups)
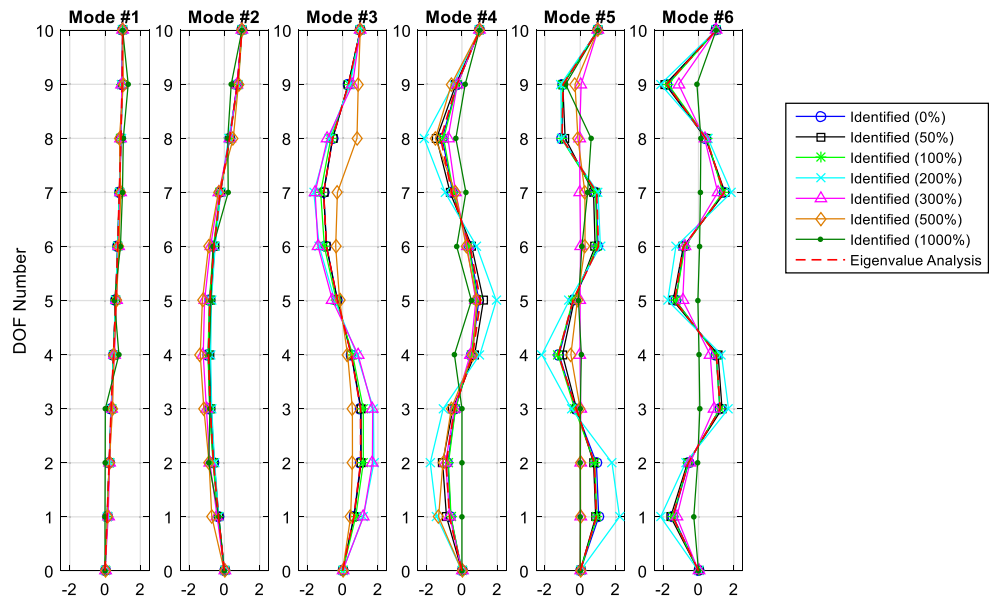
behavior of the performed methodology in the presence of the measurement noise. To do so, the frequency bandwidth for each mode has been determined from the auto-spectral density functions by the half-power bandwidth method. The lower and upper frequency ranges are selected at which the amplitudes are equal to $1/\sqrt{2}$ times the peak amplitude. The resulting frequency bandwidths are as follows; for the first mode: 2.54–2.60 Hz, for the second mode: 7.12–7.20 Hz, for the third mode: 11.55–11.63 Hz, for the fourth mode: 15.98–16.05 Hz, for the fifth mode: 19.73–19.80 Hz, and for the sixth mode: 23.54–23.62. The coherence values are averaged over the corresponding ranges.

With the calculated mean values for the selected DOF, the change in coherence with the noise level has been illustrated

for the resonant frequency bandwidths of the first six modes in Fig. 11. The value of the coherence at the resonant frequencies is decreasing as the mode number increases and/or the noise level increases. Further, it is observed that the coherence value is decreasing with the increase in the DOF number. This is an expected phenomenon because the synchronization of setups located far from the reference setup may involve larger amounts of additive error.

According to the second investigation, coherence functions have been calculated between the 1st DOF and the remaining DOFs of the structure, before and after the synchronization process. The target is to observe whether the correlations between the DOFs reach an acceptable level with the performed methodology. To this end, the 1st DOF of the structure has been selected as the reference DOF since it stays on Setup #1

Fig. 9 Comparison of the first six mode shapes of the numerical model (obtained by full measurements)
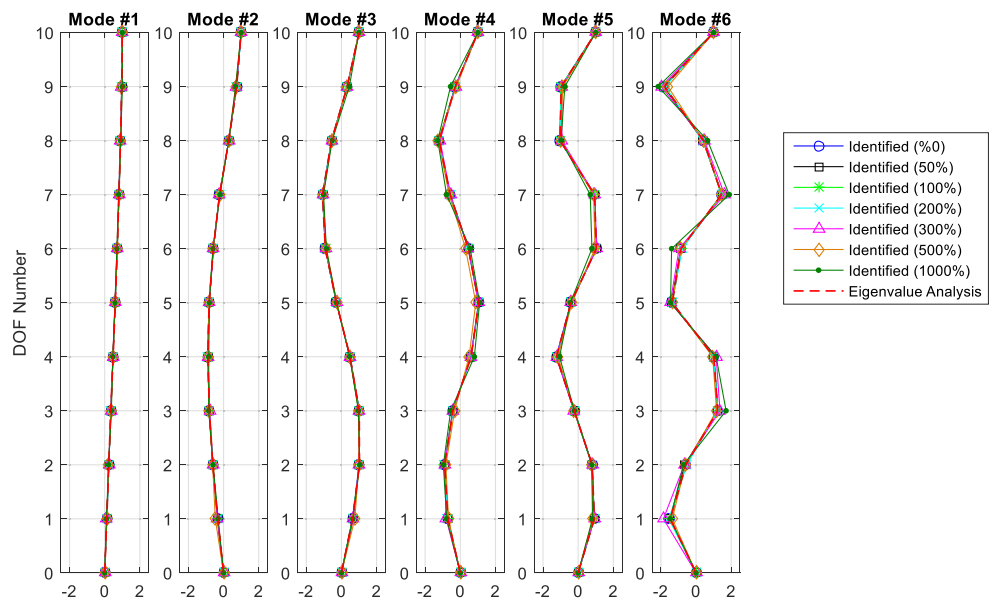
Table 3 MAC values between the results of the identifications and the eigenvalue analysis

Noise Level	Mode Number						
		1	2	3	4	5	6
0%	synch	1.0000	0.9999	1.0000	0.9985	0.9959	0.9998
	full	1.0000	1.0000	1.0000	1.0000	1.0000	1.0000
50%	synch	1.0000	0.9988	0.9998	0.9957	0.9908	0.9992
	full	1.0000	1.0000	1.0000	1.0000	1.0000	1.0000
100%	synch	0.9999	0.9997	0.9973	0.9961	0.9971	0.9989
	full	1.0000	1.0000	1.0000	0.9999	0.9999	1.0000
200%	synch	0.9999	0.9947	0.9712	0.9584	0.8900	0.9905
	full	1.0000	1.0000	1.0000	0.9997	0.9997	0.9997
300%	synch	0.9976	0.9827	0.9724	0.9536	0.1281	0.9789
	full	1.0000	0.9999	0.9999	0.9997	0.9995	0.9990
500%	synch	0.9945	0.9652	0.4301	0.9171	0.5725	–
	full	0.9730	0.9993	0.9998	0.9982	0.9993	0.9974
1000%	synch	0.9399	0.9424	–	0.1840	0.1750	–
	full	0.9991	0.9980	0.9961	0.9840	0.9882	0.9812

(reference setup) and its response signal remains unchanged after the synchronization process. The coherence functions between the response signal of the reference DOF and the response signals in each setup have been calculated before and after the synchronization process. As explained in the first investigation, coherence values have a high variation over the full frequency range. Therefore, mean coherence values have been calculated at the dominant frequency bandwidths. The same frequency ranges with the first investigation have been selected for the frequency bandwidths. This study is also performed for the aforementioned levels of measurement noise for the first six modes. The calculated absolute mean coherence values before and after the synchronization process have been illustrated in Fig. 12 for different measurement noise levels. It should be noticed that the unsynchronized values accumulate on the lower part of the figures and generally have a coherence value of 0.2 or lower.

Due to different ambient vibrations and signal noise in different setups, the low coherency before the synchronization process is as expected. It can be observed that the mean coherence in any single setup have low but almost constant values for low noise levels (0–100%), which may show that the signals in a single setup are coherent with each other. Before the synchronization process, mean coherence values between the reference DOF and the DOFs in each setup have low values which do not exceed 0.24. After the synchronization process, the mean coherences are uprising. As the number of successive setups increases, the coherency decreases. For noise levels of 0%, 50%, and 100% the coherency between all DOF remains almost constant and the minimum value is about 0.75. For this range of noise levels, the synchronized signals from all setups appear to have the same amount of coherence value for a constant noise level. This relation is repeatedly
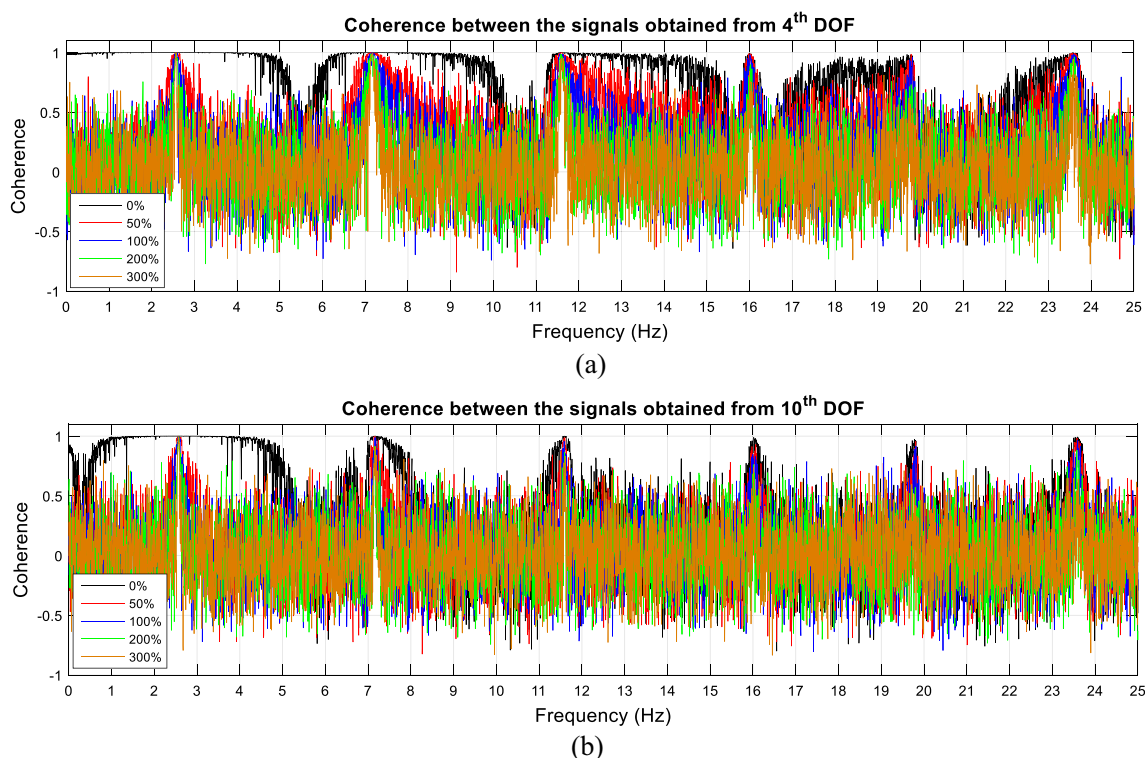
Fig. 10 The real part of the coherence functions of the signals obtained from a representatively selected DOF
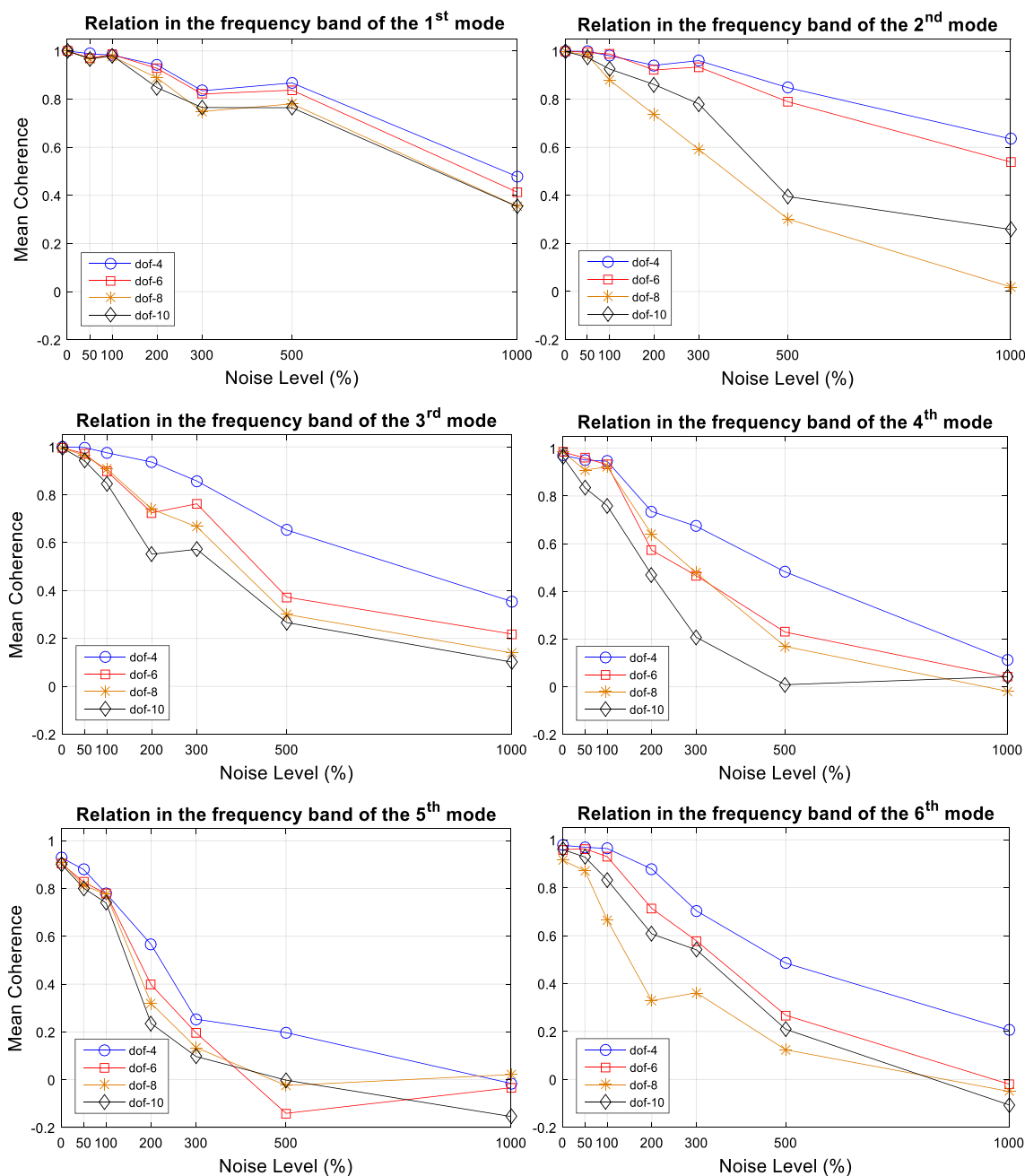
Fig. 11 Relation between the mean coherence and different noise levels for the first six modes

obtained by the selection of different noise seeds. Considering this fact, one may conclude that noise reduces the quality of the measurement leading to lower coherency values. Further, against a common believe, synchronization among the setups does not affect the coherency value. Therefore, modal properties that are calculated by using synchronization of multiple setups are expected to be dependable for noise levels less than 100%.

For comparison, Fig. 12 involves the response of the coherence of the full measurement #1 with 1000% noise. At this noise level, the coherence value between 1st DOF and 3rd DOF gets as low as 0.18 for the fifth mode. It can be seen in the figure that the synchronized data with noise levels up to 300% lead to higher coherence values than this full measurement data set. This means that even with a full measurement and high noise, the resulting data quality may be lower than that of the synchronized data obtained from multi-setup measurements. Further, the coherency values between 1st DOF and the remaining ones do not show significant change as more transformations are conducted between the measurements of interest. This is in particular importance since modal coordinates are determined with respect to a reference DOF.
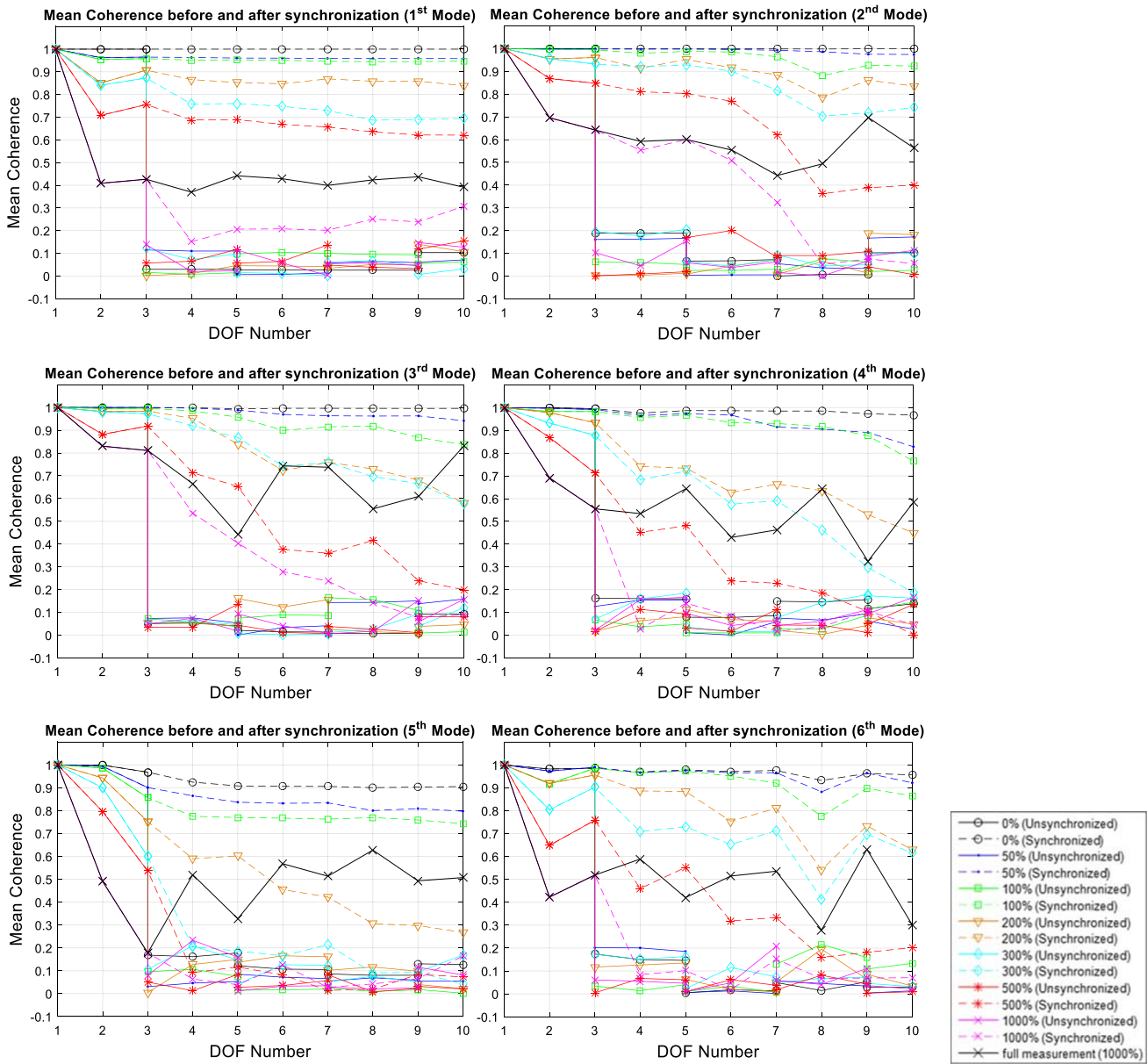
Fig. 12 Absolute mean coherence values for each DOF before and after the synchronization process

To see the effect of the length of the time histories on the coherence values, 15, 30, 45 and 60-min measurements are numerically analyzed. As the measurement length increases, it is well-known that identification quality improves. In the same respect, the coherence function is found to improve, and the mean coherence values at the resonant frequencies increase.

Discussion of the Results and Remarkable Findings

According to Fig. 9, it is seen that all the six mode shapes have been successfully identified for every noise level by using the full measurements. Therefore, it can be concluded that the misidentification of the mode shapes in Fig. 8 must be due

to the synchronization process. Up to noise level of 100%, all the six mode shapes identified by using the synchronized measurements are well matched and their MAC values are within the acceptable limit (which is accepted as greater than 0.95). For the noise levels higher than 100%, the quality of the mode shapes obtained by the synchronization is decreasing. For the noise levels of 200% and 300%, it is prominently seen that all the mode shapes, except the fifth one, are successfully identified. Here, it needs to be pinpointed that the 3rd DOF, which is used as the reference DOF, is close to a nodal point in the fifth mode. Although a proper transformation is not expected for this modal shape, the results show that up to 100% noise levels, the fifth modal shape can be successfully identified. When the coherency results of the fifth mode have been

checked from Fig. 11, it is seen for the noise levels of 200% and 300% that the coherence values are relatively lower than those of the other modes. The same result can be clearly deduced by checking the lower coherence values of the fifth mode on Fig. 12 for the same noise levels. Here, low coherence value means that the sensor placement of this numerical study is not convenient for a good identification of the fifth mode while it seems convenient for the identification of the remaining modes of interest. For the noise levels of 500% and 1000%, again the fifth mode shape have unacceptable MAC values. For the noise level of 1000%, the first two mode shapes have MAC values that are very close to the acceptance limit while the other mode shapes could not be identified. By checking the results of the noise level of 1000% on Fig. 11 and Fig. 12, it can be seen that the higher modes which could not be identified have relatively lower coherence values.

These results show that coherence investigation can be used as a tool to decide for the optimal sensor locations to identify the desired modal shapes.

Experimental Application

The data acquisition system consists of a laptop computer with a 1.5 GHz single CPU and Linux operating system, a 16-channel USBDUX-Sigma data acquisition box with 24 bit analog to digital conversion chip, a total of four piezoelectric accelerometers which have a sensitivity of 1000 mV/g and 11.4 $\mu g/\sqrt{Hz}$ spectral noise, a constant current supply for the accelerometers and a first-order low-pass filter with a cut-off frequency of 120 Hz for each channel as an anti-aliasing filter. The data acquisition system has been illustrated in Fig. 13(a). In the experimental implementation, the existing

10-story shear frame structure has been tested indoor at the base floor of the main laboratory building. The model has been placed in a corridor between two open doors as shown in Fig. 13(b) and ventilating fans of the main laboratory building are operated, which results in an air stream through the doors.

In this experimental study, a simultaneous measurement (measurement of all 10 DOFs at the same time) of the structure could not be obtained since the number of available accelerometers is not enough. Therefore, identification results of multi-setup measurements (performed by using the investigated methodology) could not be compared with the results of any simultaneous measurements. Instead, the structure has been measured by three different multiple setup configurations. Sensor placements of these configurations have been presented in Table 4. Here, Config-I represents the configuration with a fixed-reference sensor placement at the 10th DOF. This configuration has been conducted as the reference measurement for the validation of the results of roving reference sensor configurations. Config-II and Config-III represent the configurations with a roving reference sensor placement. They are considered to investigate the effect of different numbers of setups and sensor configurations on the merging procedure. Identification results of the roving reference sensor configurations, where the noise accumulation between setups is expected, have been compared with results of the fixed reference sensor configuration, where the noise accumulation between setups does not occur. In addition, results of the roving sensor configuration with five setups (Config-III) have been compared with the results of that with three setups (Config-II) in order to see the effect of noise accumulation.

For all setups in all configurations, measurement data have been acquired with a sampling frequency of 1000 Hz for

Fig. 13 (a) Data acquisition system and (b) shear frame structure (measurement of setup number #3 in Config-I)

(a)   (b)
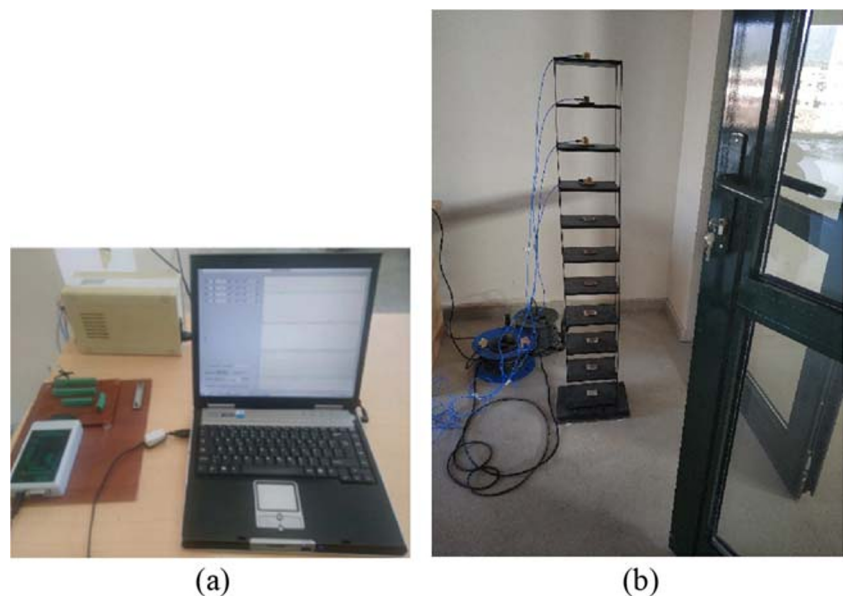
Table 4   Sensor configurations of multiple setups

Setup Numbers	Measured DOFs		
	Config-I (Reference)	Config-II	Config-III
1	1, 2, 3, 10	1, 2, 3, 4	1, 2, 3
2	4, 5, 6, 10	4, 5, 6, 7	3, 4, 5
3	7, 8, 9, 10	7, 8, 9, 10	5, 6, 7
4	–	–	7, 8, 9
5	–	–	9, 10

15 min. In order to get rid of the DC component in the signals, a fourth-order digital high-pass filter with a cut-off frequency of 0.5 Hz has been applied on each measured signal. In this experimental study, the data preparation has been done in the similar manner as in the numerical study. Maximum singular value (SV) spectra of the acceleration responses obtained from each setup have been presented for each sensor configuration in Fig. 14.

Compared to the spectral plots of the numerical study, two extra peaks are observed at the frequencies of 15.60 Hz and 23.40 Hz in all the singular value spectra. To investigate whether these peaks belong to the modes of the building on which the test structure has been located, additional acceleration measurements have been performed by placing the sensors on different locations of the main laboratory building. The auto-spectral density functions of the acceleration responses obtained from the building have been provided in Fig. 15. According to these plots, the excited natural frequencies of the main building seems to be approximately at 6.60 Hz, 13.30 Hz, 20 Hz, 23.41 Hz and 23.97 Hz. Therefore, the peak at the frequency of 23.40 Hz in the singular value spectra of the acceleration response obtained from the test structure is considered to belong to the main building. On the other hand, it seems that the building has no modes at a frequency of 15.60 Hz. At this stage, it comes to mind that this mode might belong to the test structure. However, the numerical model of the test structure has also no translational modes at this frequency in the weak direction. Further, a 3D finite element model of the test structure is formulated, and the first

(a)

(b)   (c)
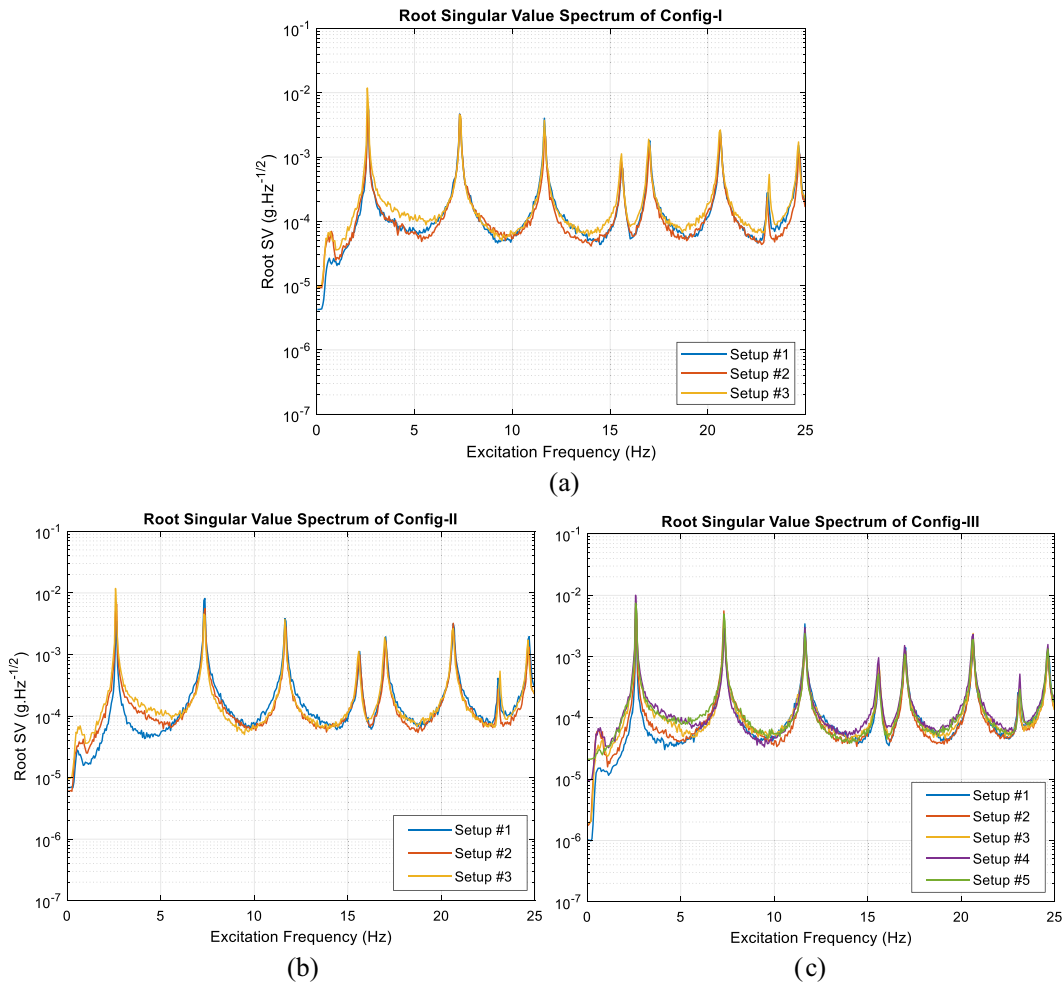
Fig. 14   Maximum root-singular value spectra of all setups in each sensor configuration
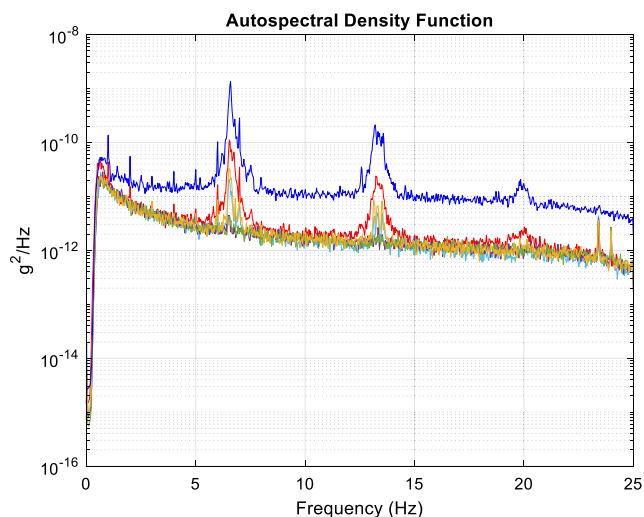
Fig. 15 Auto-spectral density plots of the acceleration measurements acquired from the main laboratory building

ten modes correspond to translational modes along the weak direction. The higher modes have frequencies that are larger than 35 Hz. As a consequence of these facts, the peak at 15.60 Hz has not been regarded in this study.

Identification Results of the Experimental Model

Modal parameter identification of the structure has been performed by using each sensor configuration. Three different well-known identification methods are implemented on the data which are merged with the investigated pre-identification (Pre-ID) merging strategy. The aim is to identify if the results depend on the identification methods or not.

As a first step, the fixed-reference multi-setup data obtained from Config-I have been employed in Bayesian Mode Shape Assembly (BMSA) technique [27]. BMSA technique is a post-identification (Post-ID) merging procedure, which gives the global modal parameters with a merging operation after the identification process. Thus, the modal frequencies, damping ratios and modal shape results have been obtained independently from the investigated Pre-ID merging procedure, and they are used as reference values for comparison.

As a second step, synchronized response data from Config-II and Config-III have been obtained by the investigated Pre-ID merging procedure and they are evaluated by using three different identification methods, which are NExT-ERA, Covariance-based Stochastic Subspace Identification (SSI-COV) method [28, 29] and Bayesian Fast Fourier Transform Approach (BFFTA) [30, 31].

In Table 5, the modal frequencies and modal damping ratios of the first six translational modes identified from Config-II and Config-III are compared with those of reference case. According to the results, the first six modal frequencies of the model identified by the investigated Pre-ID methodology have a very good agreement with the ones identified by the

reference case. Further, damping ratio identification results of all the methods, however, is slightly different from the impulse response estimation results obtained for numerical analysis (see Table 1 for comparison). Besides, the damping ratio identifications have slightly scattered results among different identification techniques. Observing the general trend of the results, the damping ratio identification obtained by the investigated Pre-ID methodology has compatible values with those of the reference case.

First six mode shapes of the physical model, which are identified from Config-II and Config-III, are presented in Fig. 16 and Fig. 17, respectively. Mode shapes which are identified from each identification method have been compared with the reference configuration of Config-I. It can be concluded that no important difference between the mode shapes is present. To investigate the quality of the mode shapes identified by the investigated Pre-ID merging strategy, MAC values have been calculated between the mode shapes that are identified from the reference configuration and, from Config-II and Config-III. These results are presented in Table 6. It has been observed that all calculated MAC values (except the 4th mode of SSI-COV in Config-III) have been obtained in the range of 0.98–1.00, which shows a high consistency of the identified mode shapes. The 4th mode shape of the analysis that is performed with the SSI-COV algorithm in Config-III has the lowest MAC value of 0.9589. Besides, NExT-ERA and BFFTA have resulted in high MAC values for the corresponding mode. Therefore, this low MAC value is considered to be related to the identification methodology. Although this mode has the lowest value, it is still in the range of acceptable limits.

The modal identification results obtained from the experimental analysis are slightly different from the results of the eigenvalue analysis of the numerical model. It can be deduced from here that the numerical and physical structure are slightly different from each other probably because of using the nominal values of geometrical and material properties in constructing the numerical model.

Coherency Investigation in-between Setups (Experimental Study)

Since a full measurement of the structure is not available, coherence functions have been calculated only between the synchronized signals and the 1st DOF, as in the second investigation of the numerical model. The coherence functions between the response signal of the 1st DOF and the response signals in each setup, before and after the synchronization process, have been calculated for each configuration. As in the numerical study, high variation in the coherence values has been observed over the full frequency range, except near the resonant frequencies.

Table 5 Identified modal frequencies and modal damping ratios of the physical structure

# Mode	Config-I (Reference) Post-ID		Config-II Pre-ID						Config-III Pre-ID					
	BMSA		NExT-ERA		SSI-COV		BFFTA		NExT-ERA		SSI-COV		BFFTA	
	f	ξ	f	ξ	f	ξ	f	ξ	f	ξ	f	ξ	f	ξ
1	2.61	0.22	2.62	0.26	2.62	0.25	2.62	0.27	2.61	0.25	2.61	0.25	2.61	0.22
2	7.33	0.20	7.33	0.15	7.33	0.16	7.34	0.16	7.33	0.25	7.33	0.25	7.32	0.22
3	11.65	0.17	11.66	0.21	11.66	0.22	11.66	0.21	11.64	0.18	11.64	0.17	11.64	0.18
4	17.00	0.19	17.03	0.21	17.03	0.33	17.03	0.20	17.01	0.19	16.99	0.24	17.01	0.21
5	20.63	0.15	20.66	0.14	20.66	0.16	20.66	0.15	20.64	0.14	20.64	0.12	20.65	0.23
6	24.65	0.10	24.68	0.12	24.68	0.15	24.68	0.14	24.66	0.17	24.66	0.17	24.65	0.15

Similar to the numerical study, a mean value of the coherence has been estimated for the first six modes at a narrow resonant frequency bandwidth. For each configuration, the frequency bandwidths are selected based on the half-power bandwidth method and are presented for each mode in Table 7. The coherence values are averaged over the corresponding ranges.

The calculated absolute mean coherence values before and after the synchronization process have been illustrated in Fig. 18 for the roving reference configurations (Config-II and Config-III). For comparison purposes, the absolute mean coherence values after the synchronization process have been also presented in the same figure for the fixed reference configuration (Config-I). Similar to the numerical study, it can be observed that the mean coherence

values for the unsynchronized measurements are almost constant within each setup. This shows that the signals in a single setup have a significant coherency with each other. Before the synchronization process, mean coherence values between the reference DOF and the DOFs in each setup have low values which do not exceed 0.3. After the synchronization process, the mean coherences are uprising to a value of 0.95 and larger. This indicates that the synchronized measurements are highly correlated. In addition, the coherence value decreases at the 3rd DOF of the fifth mode for Config-II (see Fig. 18e). Here, it should be noticed that the 3rd DOF is in the same setup with the 1st DOF and there is no synchronization in-between. The reason of this result is that the 3rd DOF is close to the nodal point of the fifth mode. At this DOF of the fifth mode, the

Fig. 16 Comparison of the first six mode shapes identified from Config-II
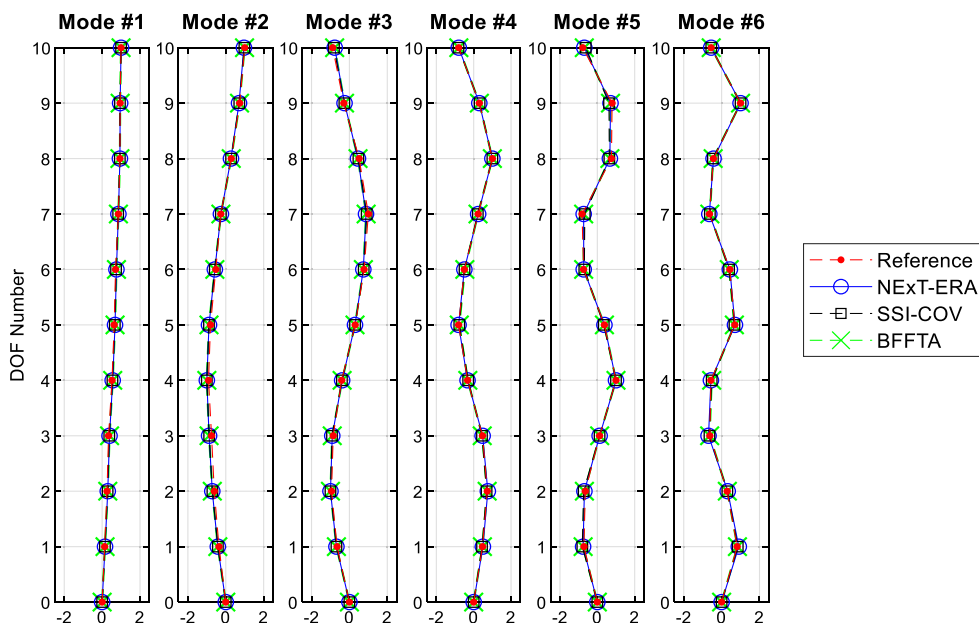
Fig. 17 Comparison of the first six mode shapes identified from Config-III
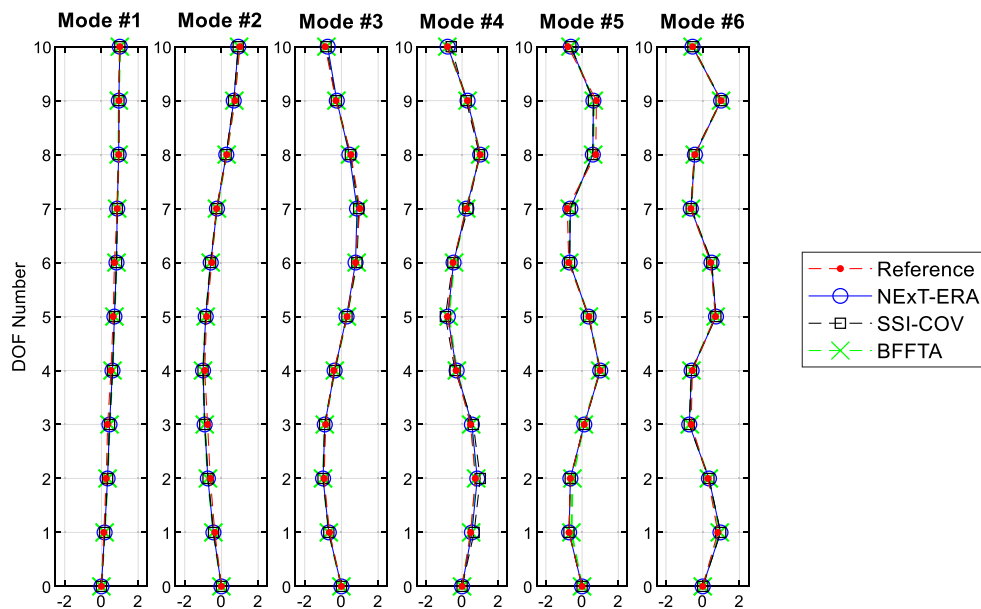
signal-to-noise ratio is lower relative to the other DOFs since the corresponding signal has a lower amplitude.

For Config-III, the coherence value decreases after the 3rd DOF of the fifth mode (Fig. 18e) which now is a reference DOF. The same behavior is seen in the numerical study since the 3rd DOF is close to a nodal point of the fifth mode and it should not have been selected as a reference DOF. Despite this fact, all the six mode shapes are successfully identified with high MAC values by using the sensor configuration of Config-III. This may show that the coherence values are not one to one related to MAC values.

Conclusions

In this study, a multiplicative frequency-domain transformation function which is an extended approach of Brownjohn [9] and Siringoringo and Fujino [10] is used for time-synchronization in the applications of OMA by using multiple setup measurements. The setups in this investigation have roving reference sensors instead of a fixed common reference among all setups. The performed procedure has been applied and verified on an existing 10 story laboratory shear frame model, and its numerical model. The coherency investigations have indicated that the synchronization procedure has considerably increased the correlation between the unsynchronized signals. The statistical properties (coherence) of the synchronized measurements compared to the full measurements appear to be alike. However, in the time domain, they are not one to one identical. Further, it has been observed that the error caused by high measurement noise appears to be unimportant for lower modes, and the error increases with higher modes. As a supportive result, the merged data of the measured multiple setups obtained in the numerical analysis lead to the exact mode shapes and frequencies in spite of the high levels of measurement noise.

Table 6 MAC values for Config-II and Config-III

# Mode	Config-II Pre-ID			Config-III Pre-ID		
	NExT-ERA	SSI-COV	BFFTA	NExT-ERA	SSI-COV	BFFTA
1	0.9985	0.9991	0.9985	0.9943	0.9942	0.9940
2	0.9935	0.9951	0.9957	0.9877	0.9879	0.9919
3	0.9928	0.9954	0.9933	0.9897	0.9960	0.9949
4	0.9997	0.9990	0.9997	0.9946	0.9589	0.9963
5	0.9948	0.9831	0.9950	0.9880	0.9875	0.9917
6	0.9980	0.9984	0.9991	0.9951	0.9939	0.9969

Table 7 Selected resonant frequency bandwidths for each configuration

Resonant Frequency Bandwidths (Hz)

# Mode	Config-I	Config-II	Config-III
1	2.60–2.62	2.60–2.63	2.60–2.62
2	7.30–7.34	7.31–7.36	7.30–7.34
3	11.62–11.67	11.63–11.69	11.62–11.67
4	16.97–17.04	17.01–17.06	16.97–17.04
5	20.61–20.65	20.63–20.68	20.61–20.65
6	24.62–24.68	24.64–24.70	24.62–24.68

The investigated Pre-ID merging strategy is proven to be unaffected by noise as long as the signal-to-noise ratio is high. Since the modal identification is performed mode by mode, the bandwidth of interest lies within the resonant frequency range, which generally has a high signal-to-noise ratio.

The performed methodology is independent from the identification technique and therefore it may be used by any modal identification method. As a general conclusion, the potential of this procedure may be its usage in large/long structures in which a fixed-positioned reference is not feasible when using a limited number of sensors and/or a single data acquisition unit.

The half-power bandwidth concept is introduced for standardization in the calculation of the mean coherence values, because the mean coherence values are found to be very sensitive to the frequency band selection.

It is observed that reference sensor locations and low signal-to-noise ratio affect the quality of the identified modal shapes. Therefore, the accuracy level of the investigated Pre-ID method depends on these two factors. Further, while a certain sensor configuration is convenient for the identification of a certain modal shape, this sensor configuration may not be suitable for the identification of another mode. Starting from this point of view, coherence investigations can be used as a tool to decide on the optimal reference sensor locations in roving sensor configurations.

Future Work

There are many sensor configuration possibilities in multi-setup measurements. The relation between the sensor configuration and investigated methodology can be broadened. Accuracy level of the methodology can be investigated by increasing the number of setups. In this case, the optimal sensor placement should be considered. Otherwise, a random increase in the number of setups will result in just a subset of all possible results. Further, a generalized optimization algorithm may be proposed for the Pre-ID data synchronization which is based on optimal sensor configuration and optimal locations of reference sensors. While doing this, coherence functions can be included in the optimization algorithm to decide for the better configuration. Here, the aim should be the identification of large number of high-quality modal shapes. In addition, the effect of closely spaced modes needs to be investigated. The magnitudes at the excitation frequencies for the various setups are generally different. Therefore, the closely spaced modes will be excited in different proportions, leading to an incorrect transformation function.

References

1. Basten THG and Schiphorst FBA (2012) Structural health monitoring with a wireless vibration sensor network. *Proc. Int. Conf. Noise Vib. Eng. ISMA 2012 17-19 Sept. 2012 Leuven Belg., pp. 3273–3283*
2. Peeters B, Guido R (1999) Reference-based stochastic subspace identification for output-only modal analysis. Mech Syst Signal Process
3. Reynders E, Roeck GD (2008) Reference-based combined deterministic–stochastic subspace identification for experimental and operational modal analysis. Mech Syst Signal Process 22: 617–637
4. Van der Auweraer H, Leurs W, Mas P and Hermans L (2000) Modal parameter estimation from inconsistent data sets. *Proceedings of SPIE - The International Society for Optical Engineering.* Society of Photo-Optical Instrumentation Engineers, p. I/
5. Döhler M, Andersen P and Mevel L (2010) Data merging for Multi Setup operational Modal Analysis with Data Driven SSI. *Proceedings of the IMAC-XXVIII, 28th International Modal Analysis Conference.* France, Europe: HAL CCSD, 2010., Jacksonville, Florida USA
6. Döhler M, Reynders E, Magalhaes F, Mevel L, De Roeck G, Cunha A (2010) Pre- and post-identification merging for multi-setup OMA with covariance-driven SSI. Conference on Structural Dynamics, *Proceedings Of The International Modal Analysis Conference*, New York, Curran, pp 380 –393
7. Reynders E, De Roeck G, Magalhães F and Cunha Á (2009) Merging strategies for multi-setup Operational Modal Analysis: Application to the Luiz i steel arch bridge. *Conference Proceedings of the Society for Experimental Mechanics Series.* p. 15p
8. Mevel L, Basseville M, Benveniste A, Goursat M (2002) Merging sensor data from multiple measurement set-ups for non-stationary subspace-based modal analysis. J Sound Vib 249:719–741
9. Brownjohn JMW (2003) Ambient vibration studies for system identification of tall buildings. Earthq Eng Struct Dyn 32:71–95
10. Siringoringo DM, Fujino Y (2009) Noncontact operational modal analysis of structural members by laser Doppler Vibrometer. Computer-Aided Civil and Infrastructure Engineering 24:249–265
11. Felber AJ (1994) Development of a hybrid bridge evaluation system. Doctor of Science Thesis, The University of British Columbia, Vancouver
12. Juang J-N and Pappa RS (1986) Effects of Noise on Modal Parameters Identified by the Eigensystem Realization Algorithm. *Journal of Guidance, Control, and Dynamics.* Vol. 9(No. 3), 294–303
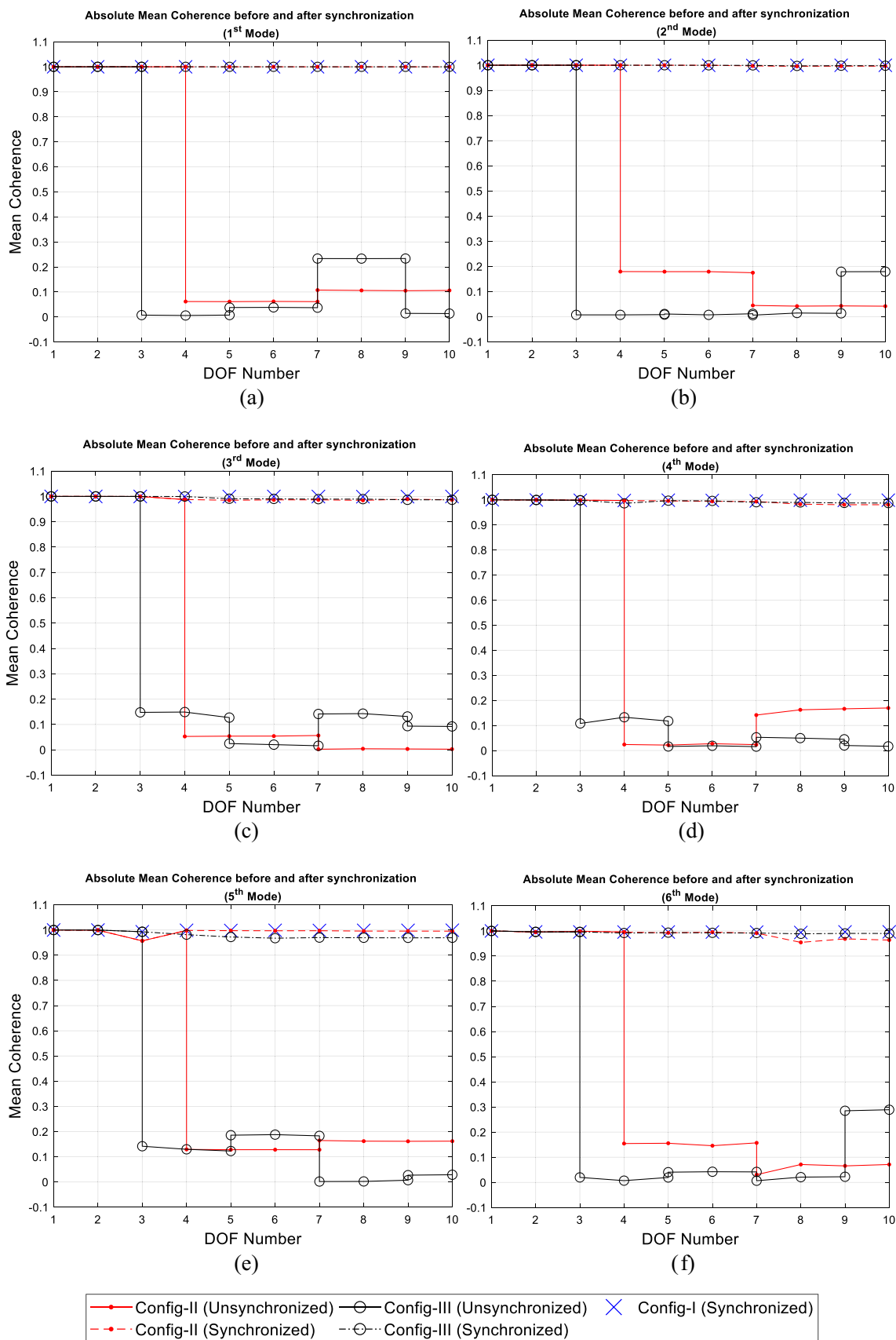
Fig. 18 Absolute mean coherence values for each DOF before and after the synchronization process

13. Zhu Y-C, Au S-K (2017) Spectral characteristics of asynchronous data in operational modal analysis. Struct Control Health Monit

14. Ceylan H (2015) Modal parameter identification of civil engineering structures by using an output-only system identification technique. Master of Science Thesis, Izmir Institute of Technology, Izmir

15. Ceylan H and Turan G (2016) Modal Parameter Identification of a Continuous Beam Bridge by Using Grouped Response Measurements. *Istanbul Bridge Conference*. 8-10 August. Istanbul, Turkey

16. Ceylan H, Turan G and Hızal Ç (2017) Modal identification with a limited number of sensors by using two different identification techniques. *4th International Conference on Earthquake Engineering and Seismology*. 11-13 October, Eskisehir, Turkey

17. MATLAB (2012). Version R2012b 8.0.0.78. The MathWorks Inc., Natrick, Massachusetts

18. Newmark NM (1959) A method of computation for structural dynamics. J Eng Mech Div 85:67–94

19. Caicedo JM (2001) Two structural health monitoring strategies based on global acceleration responses: development, implementation, and verification. Master of Science Thesis, Washington University, St. Louis

20. Caicedo JM (2003) Structural health monitoring of flexible civil structures. Doctor of Science Thesis, Washington University, St. Louis

21. Caicedo JM (2011) Practical guidelines for the natural excitation technique (NExT) and the Eigensystem realization algorithm (ERA) for modal identification using ambient vibration. Exp Tech 35:52–58

22. James GI, Carne T and Lauffer J (1993) The Natural Excitation Technique (NExT) for modal parameter extraction from operating wind turbines. *Sandia National Laboratories, Albuquerque, NM and Livermore, CA, SAND92-1666*

23. Juang J-N, Pappa RS (1985) An Eigensystem realization algorithm for modal parameter identification and model reduction. J Guid Control Dyn 8(5):620–627

24. Mahmood SMF, Haritos N, Gad E, Zhang L (2014) A multi-reference-based mode selection approach for the implementation of NExT–ERA in modal-based damage detection. Struct Control Health Monit 21(8):1137

25. Nayeri RD, Tasbihgoo F, Wahbeh M, Caffrey JP, Masri SF, Conte JP, Elgamal A (2009) Study of time-domain techniques for modal parameter identification of a long suspension bridge with dense sensor arrays. J Eng Mech 135(7):669–683

26. Moaveni B (2007) System and damage identification of civil structures. *Doctor of Philosophy in Structural Engineering*. University of California, San Diego

27. Hızal Ç, Turan G, Aktaş E and Ceylan H (2019) A mode shape assembly algorithm by using two stage Bayesian fast Fourier transform approach. Mech Syst Signal Process 134:106328

28. Overschee PV, De Moor B (1996) Subspace identification for linear systems: theory, implementation, applications. Kluwer Academic Publishers, New York City

29. Peeters B, De Roeck G (2001) Stochastic system identification for operational modal analysis: a review. J Dyn Syst Meas Control 123(4):659–667

30. Yuen K-V, Katafygiotis LS (2003) Bayesian fast Fourier transform approach for modal updating using ambient data. Adv Struct Eng 6(2):81–95

31. Au S-K (2011) Fast Bayesian FFT method for ambient modal identification with separated modes. J Eng Mech 137(3):214–226